N94-35910

MANUFACTURING AND TESTING OF A MAGNETICALLY SUSPENDED COMPOSITE FLYWHEEL ENERGY STORAGE SYSTEM

Stephen Wells
FARE Inc.
College Park, MD

Da-Chen Pang
Dr. James A. Kirk
University of Maryland
College Park, MD

ABSTRACT

This paper presents the work performed to develop a multiring composite material flywheel and improvements of a magnetically suspended energy storage system. The flywheel is constructed of filament wound graphite/epoxy and is interference assembled for better stress distribution to obtain higher speeds. The stationary stack in the center of the disk supports the flywheel with two magnetic bearings and provides power transfer to the flywheel with a motor/generator. The system operates under a 10^{-4} torr environment and has been demonstrated to 20,000 rpm with a total stored energy of 15.9 Wh. When this flywheel cycles between its design speeds (45,000 to 90,000 rpm), it will deliver 242 Wh and have a usable specific energy density of 42.6 Wh/kg.

INTRODUCTION

The flywheel energy storage system has higher specific energy density (SED), larger power output, and longer cycle life than typical battery systems for spacecraft applications [1]. The flywheel and test apparatus shown in figure 1, which was manufactured and tested, consist of the following components:

- A multi-ring interference assembled flywheel fabricated from graphite-epoxy, including two magnetic bearing return rings and motor/generator magnets.
- Two active "pancake" magnetic bearings which together form the top and bottom portions of a test apparatus (stack).
- A motor/generator mounted between the two magnetic bearings. This provides power transfer into and out of the test apparatus.
- A vacuum enclosure supporting the top and bottom of the "stack" and completely surrounding the flywheel.
- Display/control panel offering control and data acquisition of the system.

COMPOSITE FLYWHEEL

The construction of the composite flywheel cylinders by filament winding consists of four major steps. The first step is design, which includes the selection of materials, geometry of the part, and orientation of the fiber. Step two includes selection and control of conditions which are to be maintained during the manufacturing process. The third step is the machining and assembly of the flywheel. The final step involves testing the materials to determine if their strength matches theoretical values.

Flywheel Design

The flywheel energy storage system is designed to cycle between 37.5% to 75% of its maximum strength with speeds of 45,000 rpm to 90,000 rpm. This will deliver 242 watt hours and have a usable energy density of 42.6 Wh/kg.

The flywheel inside diameter and height were designed to fit within an existing test apparatus [2] and consists of two composite rings and an inner metal ring. The metal ring consists of aluminum rings for balancing, nickel iron rings for magnetic suspension, a ring containing the motor/generator magnets, and aluminum spacers. The nominal diameters of the two composite rings are 4.68 inches (118.87 mm) inside diameter and 5.6 inches (142.24 mm) outside diameter for the first ring and 6.61 inches (167.89 mm) outside diameter for the second ring. FLYANS code was used to determine optimal composite ring dimensions to produce favorable stresses [3,4,5] and a 0.006 inch (0.1524 mm) interference fit was selected for the composite rings.

From micrographic tests of a preliminary composite flywheel, abnormal end effects on the microstructure were found. The effect is due to the filament winder carriage changing directions, thus the composite rings were made 0.25 inches (6.35 mm) longer on each end. The height of the first composite ring was 9.5 inches (241.3 mm) long and the second composite ring was made 0.002 inches (0.0508 mm) longer so that the top surfaces of the rings would not be flush when pressed together. The final height of the flywheel once the ends were cut off is 9 inches (228.6 mm).

Flywheel Manufacture

Two composite rings were filament wound using a Toho G40-800 carbon graphite fiber and a Shell Epon 826 epoxy resin. The rings were filament wound onto steel winding mandrels using a two-axis filament winding machine as shown in figure 2. The winding angle, α, is the angle between the axis and the fiber shown in figure 3. For the flywheel, fibers are oriented as close as possible to the tangential direction, i.e., a winding angle of 90° (for practical purposes the fiber angle is 87°). This ensures that for one revolution of the mandrel the carriage should advance one fiber bandwidth. Reversal at the end of carriage travel needs to be accurately controlled to avoid excessive build-up at the flanges of the mandrel. A precision lead screw is used to control the carriage movement. The fiber is pulled through a tensioner into the matrix bath. Wet winding epoxy resins are sufficiently low molecular weights that they are fluids at room temperature. To assist in wetting the fiber during the winding process, a 250 Watt heat lamp with temperature control was used to heat the resin. This increases resin temperature, dropping the viscosity of the resin.

Heating the resin reduces the viscosity from 100 poise to 6-7 poise, or a 93% reduction of viscosity. A disadvantage of heating the resin is that the resin bath pot life is reduced from eight hours to three hours.

Due to voids observed in digital imaging samples of filament wound parts, it was decided to integrate a vacuum bagging technique into the flywheel manufacturing process. Vacuum bagging uses air pressure to apply force around the part which consolidates the fibers, removes excess resin by trapping it in layers of bleeder cloth, and removes volatiles which produce voids.

Once the part is vacuum bagged, the mandrel is placed onto a cradle which has been fitted with bearings to allow for rotation during the curing process. The mandrel rotates to prevent collection of resin at one point and sagging of the fiber. The part is cured at 175°F for one hour to allow resin to flow, and then cured at 350°F for two hours to cure the epoxy.

Flywheel Machining and Assembly

To produce the interference fit, a 0.4 degree taper was machined on the outside surface of the inner filament wound ring creating a 73% engagement between the first and second rings. The two rings were lubricated with epoxy and then pressed together with 30,000 pounds of force. Once the rings were pressed together, 1/4 inch of material was removed from the top and bottom to give the final flywheel height of nine inches. The inside and outside diameters of the pressed composite rings were machined to designed size dimensions using standard carbide cutting tools. The aluminum balancing rings, aluminum spacers, motor return ring, and magnetic bearing rings were press fit into the flywheel with a LN1 press fit (0.0005 inch or 0.0127 mm) using a lathe end dead center. Alternating dark and light markings were painted for motor commutation and rpm sensors to complete the flywheel.

Testing of Materials

To verify the composite material properties, acid digestion, micrograph, and digital imaging tests were performed to determine void content and volume fraction, and NOL tension tests were conducted for tensile strength and composite stiffness in the fiber direction. Fiber modulus and tensile strength was 20% and 25% below theoretical. Machining generates broken fibers and cracks and the less than perfect geometry of the NOL ring specimen was suspected to contribute to these errors. Volume fraction was measured to be 62% fiber which is comparable to high performance composite materials. Void content was measured at 7% using a digital imaging technique with a non-vacuum bagged part, thus the decision to vacuum bag all future composite parts to decrease the void content.

TESTING APPARATUS

The test apparatus performs the task of containing and spinning the composite flywheel to high speeds. The test apparatus consists of two magnetic bearings for suspension of the flywheel, an electrical system to provide control and monitoring of the system, a

motor/generator to provide the means for the input and output of energy to the flywheel, and a vacuum chamber capable of 10^{-5} torr to simulate a zero atmosphere environment. A block diagram of the electrical paths of the test apparatus is shown in figure 4.

Magnetic Bearing

The magnetic bearings allow rotation of the flywheel without contacting any surfaces. Our system consists of two magnetic bearings for stability of the system. The bearing consists of a combination of permanent magnets (PMs) which provide passive support through permanent magnets in the axial direction and electromagnets (EMs) which provide active positioning control in the radial direction. The bearing is divided into four quadrants to decouple the flux produced by adjacent quadrants. The flux paths are separated into two independent axes, east-west and north-south, and each axis has its own independent control system. If the flywheel is not centered, the permanent magnets will create a destabilizing force to pull it farther off center. The control system responds to the displacement by sending a current through the EM, which results in additional corrective flux which adds to the bias flux to produce a net restoring force.

A block diagram of the magnetic bearing system is shown in Figure 5. There are four major components in the system: the magnetic bearing actuator, rotor dynamics, displacement sensors, and control system. Voltage feedback from the control system goes into magnetic bearing actuators. The actuator consists of the power amplifier, power supply, and electromagnetic coils which provide additional flux in the air gap to generate stabilized force. The power amplifier is a voltage-to-current bridge circuit design which can drive large inductive load with twice the output power. The actuator force F_c, combined with the disturbance force F_d, affect the rotor dynamics. The rotor dynamics models the mechanical system and the destabilizing force from the permanent magnet flux distribution in the radial direction. The eddy current transducers measure the displacement of the flywheel with sensor error η. Then the sensor output is fed back into the control system. The control system has a proportional and derivative compensation circuit to optimize system performance. The reference voltage input in the forward loop is used to center the flywheel. The error signal, subtracting the feedback signal from reference voltage signal, passes an adjustable gain and a low pass filter before going into the actuator. The adjustable gain is used to stabilize the system and change the magnetic bearing stiffness.

Motor/Generator

The motor/generator, located between the two magnetic bearings, converts the stored mechanical energy into electrical energy. The motor/generator is a permanent magnet, electronically commutated, ironless armature DC brushless design. The motor/generator was designed by Niemeyer [6] and was implemented by Lashley [7,8]. Motor commutation is provided by position sensors and switching transistors, which is based on the sensor measurement of the rotor position, i.e., the angular location of the magnet poles relative to the armature windings. The transistors switch the armature current to maintain a unidirectional torque. The position sensors are optical emitter-detector pairs, chosen for their small size. Speed control is provided by pulse width modulation (PWM) through an Automation Inc. LC4C motor controller [9].

Display/Control Panel

The display systems which are integrated into the energy storage system are as follows:

- Displacement
- Power amplifier voltage and current output
- Power supply voltage and current
- Percentage of PWM waveform of motor
- Vacuum of system
- Temperature of motor and magnetic bearings

The control capabilities of the system are:

- Magnetic bearing controller with adjustable stiffness and damping
- Flywheel position
- Motor speed
- Motor controller voltage

Vacuum System

To avoid windage losses during flywheel rotation, the flywheel energy storage system is placed inside a vacuum chamber as shown in figure 6. The vacuum chamber is a two piece design consisting of a vacuum chamber on an aluminum base plate sealed by a rubber gasket. Vacuum is pumped down in a two stage process. A roughing pump provides vacuum to 10^{-3} torr and a diffusion pump provides vacuum down to 10^{-5} torr. High vacuum electrical feed-throughs are used to provide power to the motor, sensor signal paths, and magnetic bearing coil power through the vacuum chamber.

TESTING AND PERFORMANCE ENHANCEMENT

Before higher speeds could be obtained by the system, several issues had to be addressed. The number of turns of the magnetic bearing actuator coil, power amplifier voltage, motor commutation, motor/controller inductance matching, system ultimate vacuum, system vibration response, system balancing, and magnetic materials limited the speed of the flywheel.

Voltage Saturation

The system had magnetic suspension failure at 6,000 rpm due to voltage saturation of the power amplifiers. To decrease the voltage demand of the EM coils, the number of turns in the actuators was decreased. Also, the power amplifiers which drive the EM coils were changed from APEX PA01 to APEX PA61 which have higher voltage and current capacities [10]. The power supply voltage was increased from 24 volts to 48 volts to

accommodate for the new power amplifiers. The power amplifiers used a voltage-current bridge design which generates twice the power of the previous design. These changes eliminated the voltage saturation issues currently, but if voltage saturation occurs again at higher speeds, it would be necessary to redesign the system using switch amplifiers.

Motor/Generator

The motor/controller combination used in our system is limited by their impedance mismatch. The Automation LC4C motor controller has a minimum inductance load of 150 μH and a suggested inductance of 1 mH [9] and the motor has an inductance value of 54 μH. The low inductance of the motor causes a high current slew rate and current saturation of the motor controller then limiting the motor speed. Methods to correct for this mismatch were to decrease the controller input voltage and add dummy inductors into the motor windings.

Motor commutation was originally provided using OPTEK OPB701 optical sensors. These sensors use a photodarlington output, which gives a higher gain but a lower response time of 1 ms [11]. Due to the slow response time, the system could not reach speeds above 15,000 rpm and thus the optical sensors were replaced by OPTEK OPB700 phototransistor sensors with a schmitt trigger. These sensors provide a response time of 0.1 ms and is enhanced by a schmitt trigger for square wave output. A comparison of the output of the two sensors and motor current is shown in figures 7 and 8.

Vacuum System

To avoid windage losses during flywheel rotation, the flywheel energy storage system is placed inside a vacuum chamber. Since windage loss is proportional to the gas density, the system can achieve high speed under vacuum [12]. Spin-down testing for our flywheel energy storage system under air and 10^{-4} torr was conducted as shown in figure 9.

Vibration Analysis

Dynamic analysis performed on our system showed a significant undamped resonance at 5400 rpm. Since the structure itself is very stiff, modes below approximately 300 Hz are due to mounting stiffness of the structure. The effective mounting stiffness was reduced by the use of rubber pads under the feet of the stack and of the vacuum chamber. A repeat modal test showed that the mode disappeared and all of the rigid-body modes of the structure were much lower. It is also theoretically possible to increase the stiffness and push the modes up the frequency scale, but this is more difficult in practice.

Balancing

For the high speed of rotation, the mass balancing of the flywheel becomes very important. In-situ balancing methods had originally been adopted for our flywheel system from Bruel & Kjaer data [13]. Initial experiments gave poor results due to the larger than

anticipated third harmonic content of the measured vibration signal. Attempts were made to commercially balance the flywheel. Since the flywheel does not have a shaft, which is required by balancing machines, a precision ground shaft and precisely machined collars were used to set up the center for balancing. Even though the flywheel/shaft/collar assembly was balanced as accurately as possible, the vibration increased when the flywheel spin tested. It was concluded that it is not possible to recreate the magnetic bearing center using mechanical fixtures for balancing, and all balancing must be done in-situ. A final attempt at balancing was made, using trial and error procedures, by observing the X-Y orbit of the flywheel and adding or subtracting small weights to make this orbit smaller, which produced desirable results.

For a composite flywheel, balancing is a difficult issue because it is undesirable to drill holes within the composite part. To circumvent this problem, a thin aluminum ring is pressed into the composite and set screw holes were drilled every 30 degrees. Weight is changed by adding or removing set screws from the aluminum ring. For the composite wheel, it was found that only a few grams of added weight were necessary to achieve the proper balance for the flywheel.

Third Harmonic Noise

A large third harmonic component was measured in the displacement signal causing a diamond shaped X-Y orbit as shown in Figure 10 as compared to a displacement signal without the third harmonic shown in Figure 11. This third harmonic noise is undesirable because it requires more control voltage and current and the system is more difficult to balance. From testing different batches of return rings, it was found that the third harmonic noise was caused by magnetic material saturation. The magnetic bearing return rings are made of Carpenter High Permeability 49% nickel iron material which has a magnetic saturation value of 1.2 Tesla [14]. Most magnetic properties quoted for this material are for thin laminations. Solid materials utilized in our system may present non-uniform properties after heat treatment processing. The preliminary magnetization test suggested that the solid material has the same magnetic saturation value but much lower permeability and higher core losses.

DISCUSSION AND CONCLUSIONS

The manufacturing process and testing for a composite flywheel has been sucessfully conducted. The magnetically suspended composite flywheel energy storage system has been developed and reached the speed of 20,000 rpm. In the process to achieve higher speed, the problems of voltage saturation, vibration, motor commutation, and balancing have been solved. Additional R&D is necessary before commercialization of the final prototype. A new motor and motor controller design is necessary to reach higher speeds, and further magnetic modeling and testing of the magnetic bearings should be performed to eliminate the third harmonic noise.

ACKNOWLEDGMENT

This work was supported by NASA Goddard Space Flight Center contract NAS5-31704 under supervision of Ernie Rodrigues and Bob Beaman. I would also like to thank

Chris Lashley and Bob Linkins from the University of Maryland, and John Chandler from Automotion Inc. for their technical support.

REFERENCES

1. Kirk, J.A., Anand, D.K., Satellite Power Using a Magnetically Suspended Flywheel Stack, Journal of Power Sources, Vol. 22, pp. 301-311, 1988.
2. Magnetically Suspended Flywheels for Inertial Energy Storage, Final Report, NAS5-30091, 1991.
3. Ries, Douglas M., Manufacturing Analysis for a Composite Flywheel, M.S.Thesis, University of Maryland, 1990.
4. Kirk, J.A., Ries D.M., Manufacturing Analysis of Composite Mulit-Ring Flywheel, Aerospace Engineering, October 1992, pp. 14-18.
5. Kirk, J.A., Anand, D.K., Overview of a Flywheel Stack Energy Storage System, Proceedings of the 23rd Intersociety Energy Conversion Engineering Conference, July 31 to August 5th, Denver, Colorado, 1988.
6. Niemeyer, W.L., Design of a High-Efficiency Motor/Generator for Flywheel Energy Storage, M.S. Thesis, University of Maryland, 1988.
7. Lashley, Christopher, Development of a High-Efficiency Motor/Generator for Flywheel Energy Storage, M.S. Thesis, University of Maryland, 1991.
8. Lashley, C., Anand, D., Zmood, R. B., Development of a High-Efficiency Motor/Generator for Flywheel Energy Storage System, 26th Intersociety Energy Conversion Engineering Conference, 1991.
9. Automation, Inc., Model LC-4 Users Manual, Ann Arbor, Michigan, 1988
10. Apex Microtechnology Corporation, APEX Hybrid & IC Handbook, Tucson, Arizona, 1991.
11. Optek Technology, Inc., OPTEK Optical Sensors Handbook, Carrollton, TX, 1993.
12. Dugger, G.L. et al, Heat-Engine/Mechanical-Energy-Storage Hybrid Propulsion Systems for Vehicles, John Hopkins University Applied Physics Laboratory, 1972.
13. Broch, J.T., Mechanical Vibration and Shock Measurements, Bruel and Kjaer Measuring Systems Inc., Naerum, Denmark, 1973.
14. Carpenter Technology, Soft Magnetic Alloys, Carpenter Technology Brochure, 1991.

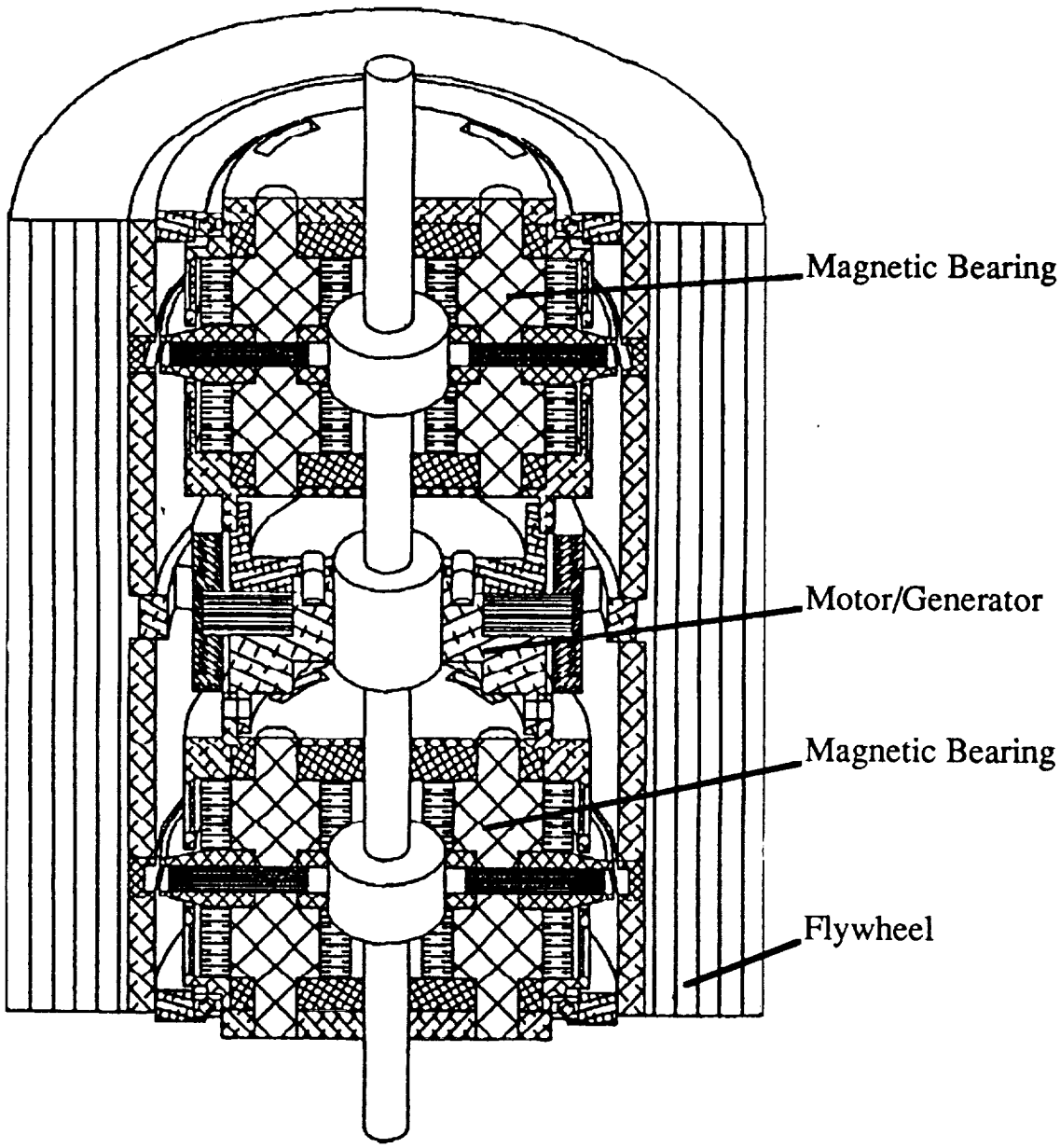

Figure 1. Magnetic Bearing System

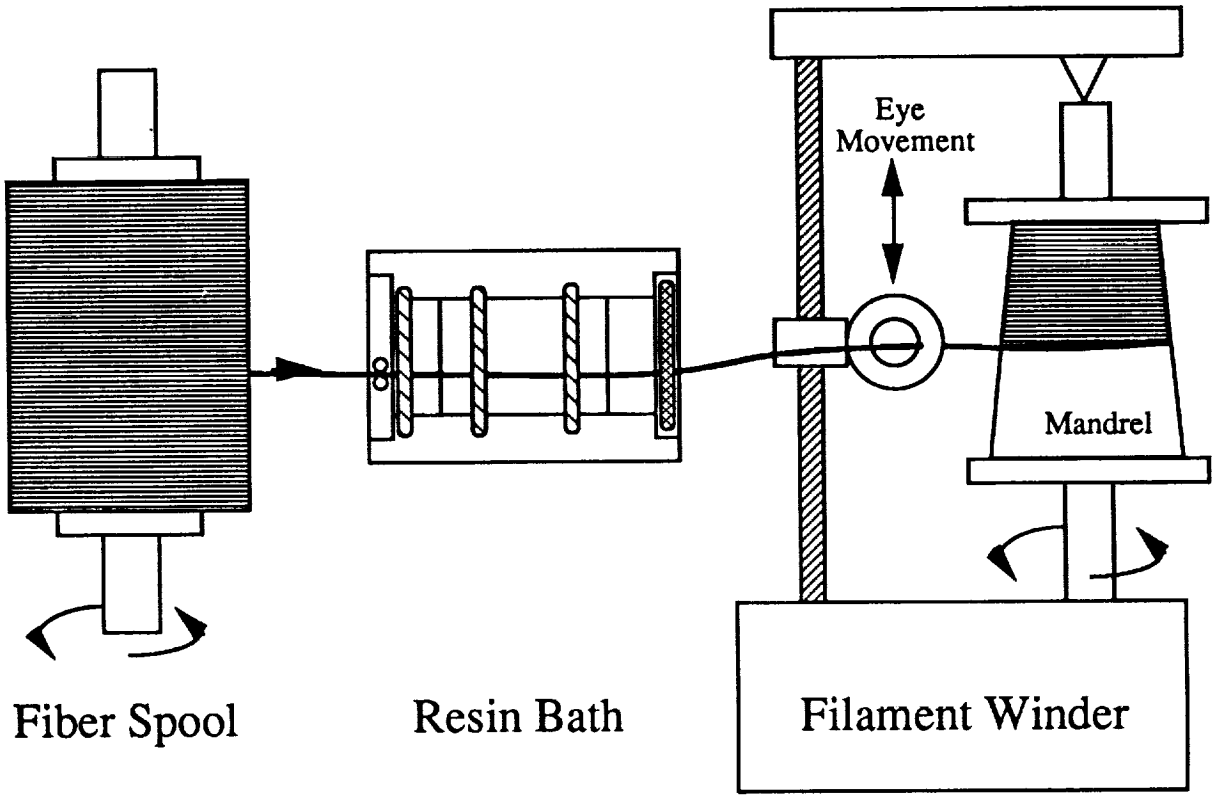

Figure 2. Two-Axis Filament Winding Process

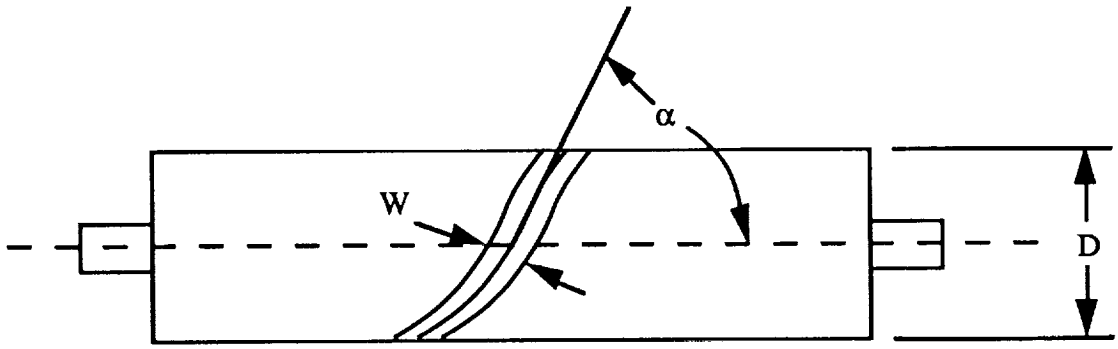

Figure 3. Wind angle

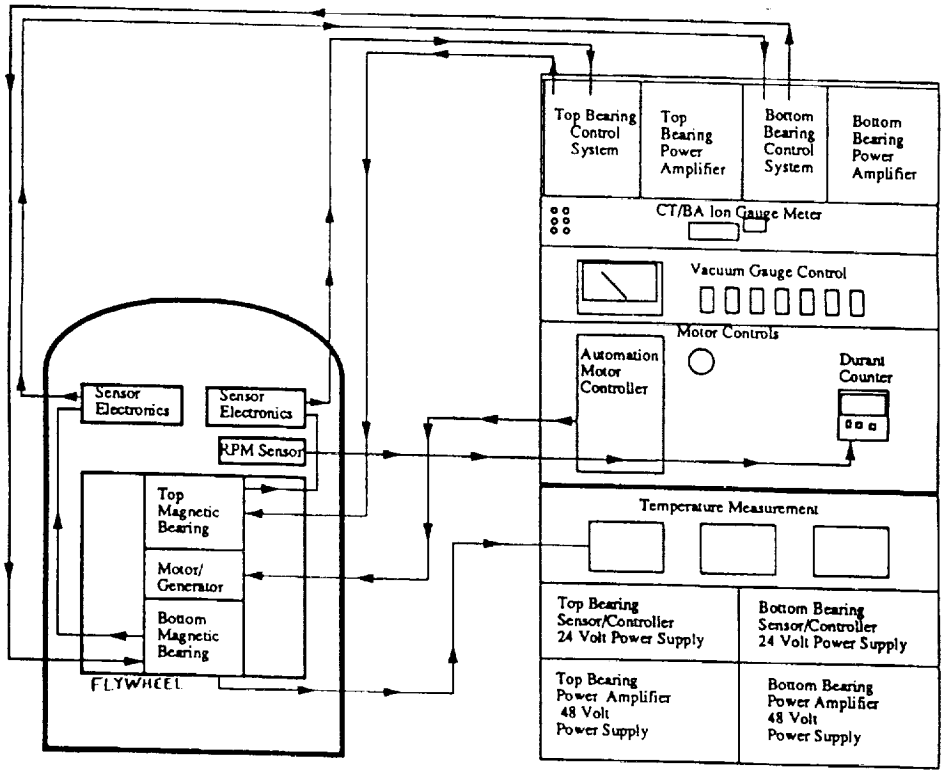

Figure 4. Magnetic Bearing Electronic Setup

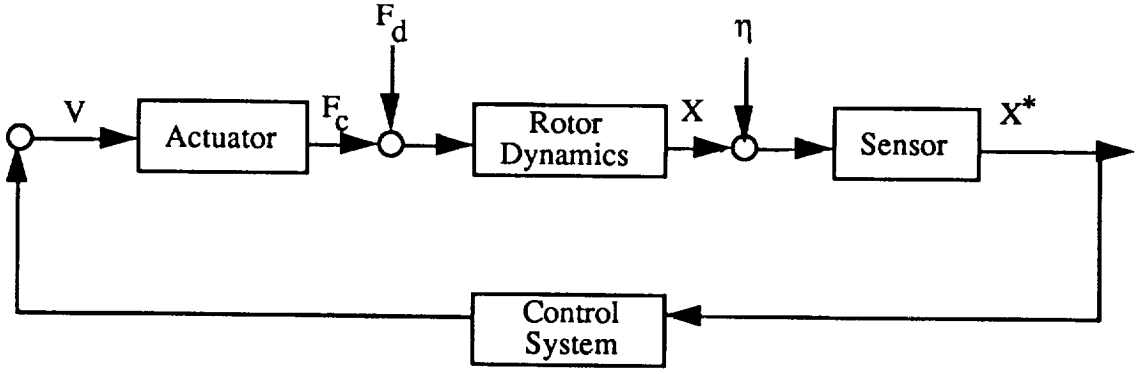

Figure 5. System Block Diagram

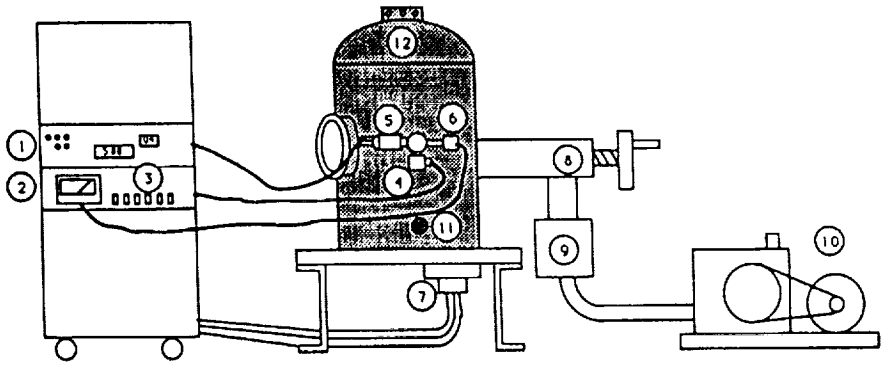

1 CT/BA Ionization Gauge Control for 10^{-5}Torr system
2 Hastings Vacuum Gauge Control for 10^{-3}Torr system
3 Vacuum control switches
4 Emergency vent valve
5 Ionization Gauge
6 Hastings Vacuum Gauge
7 Vacuum feedthroughs (Electrical wires through vacuum chamber)
8 Vacuum chamber valve$_5$
9 Diffusion pump for 10^{-5} Torr system
10 DuoSeal Model 1402 Vacuum Pump for 10^{-3}Torr system
11 Available port for cold trap (to remove water vapor)
12 Vacuum chamber

Figure 6. Vacuum Chamber Setup

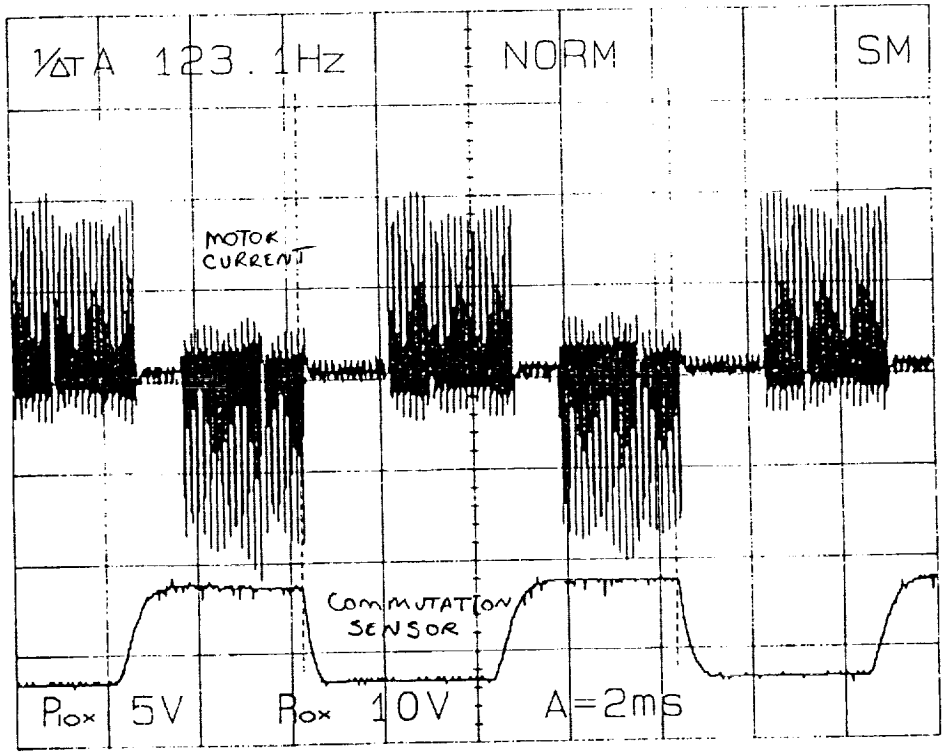

Figure 7. Photodarlington Optical Sensor Output

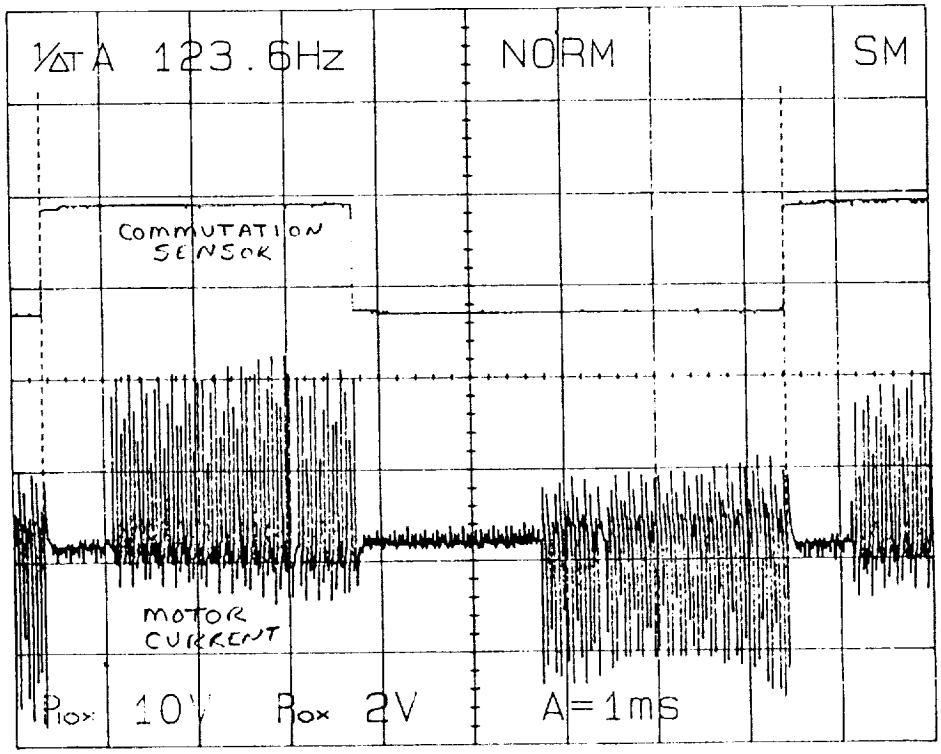

Figure 8. Phototransistor Optical Sensor Output

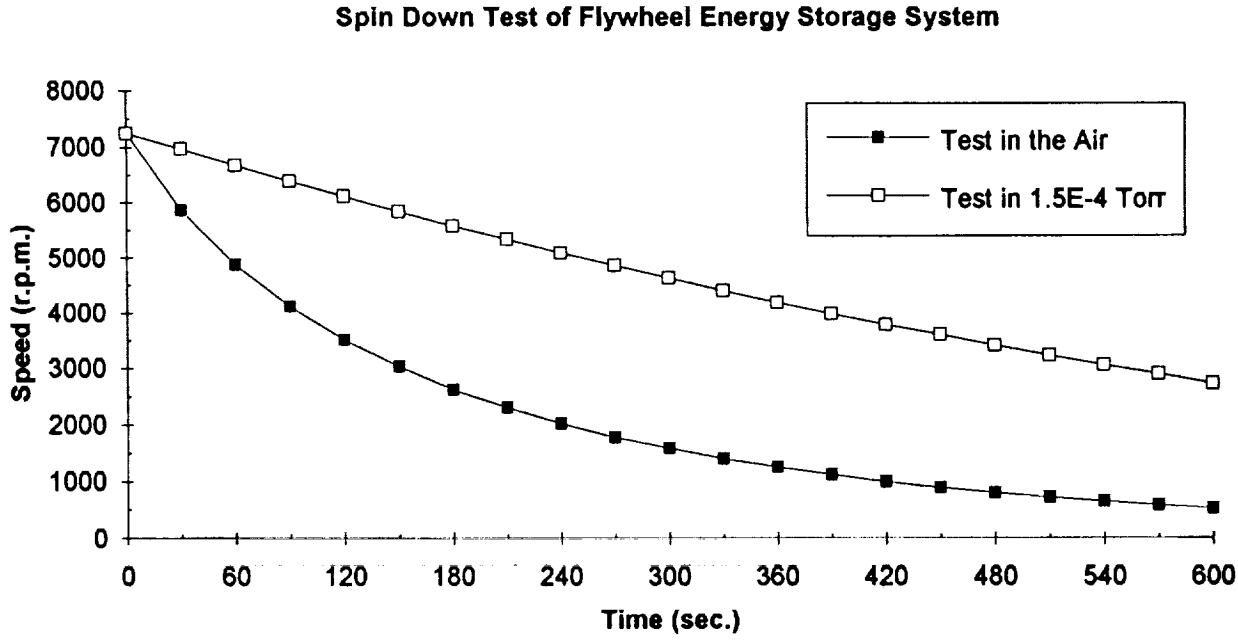

Figure 9. Spin-down Tests of the Energy Storage System in Air and in Vacuum

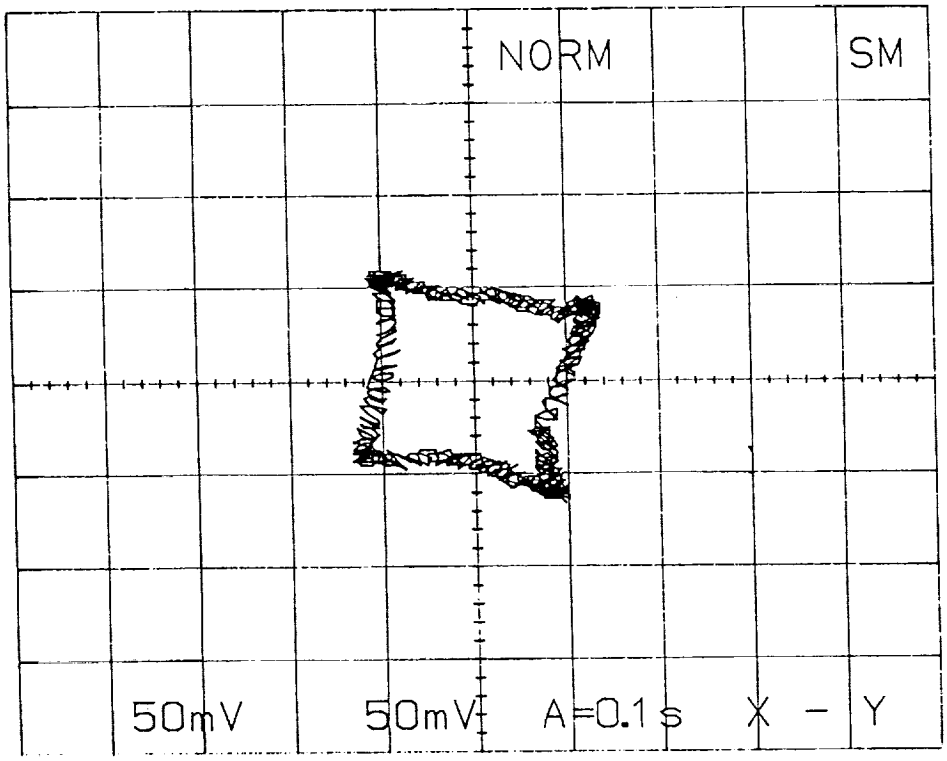

Figure 10. X-Y Orbit with Third Harmonic Present

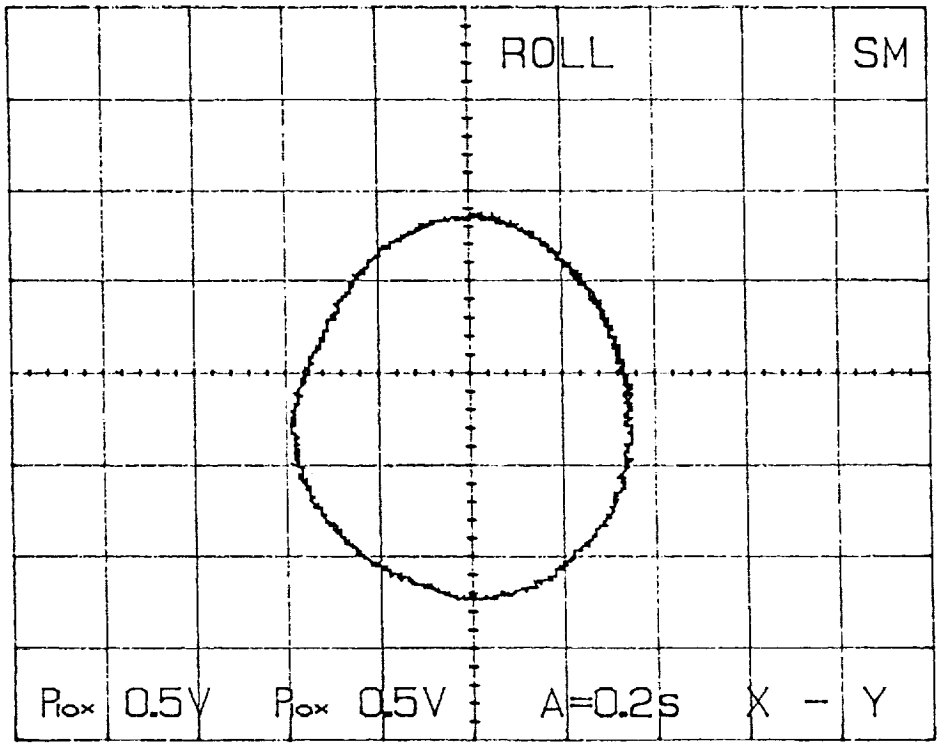

Figure 11. Normal X-Y Orbit